High-quality frozen extracts of *Xenopus laevis* eggs reveal size-dependent control of metaphase spindle micromechanics

Jun Takagi[a] and Yuta Shimamoto[a,b,c,*]
[a]Quantitative Mechanobiology Laboratory, Center for Frontier Research, National Institute of Genetics, Mishima, Shizuoka 411-8540, Japan; [b]Department of Genetics, School of Life Science, SOKENDAI, Mishima, Shizuoka 411-8540, Japan; [c]PRIME, Japan Agency for Medical Research and Development, Tokyo 100-0004, Japan

ABSTRACT **Cell-free extracts from unfertilized *Xenopus laevis* eggs offer the opportunity for a variety of biochemical and biophysical assays for analyzing essential cell cycle events such as metaphase spindle assembly. However, the extracts often exhibit substantial variation in quality and have low storage stability, factors that hamper their experimental utility. Here we report a simple two-step method for preparing frozen egg extracts that retain spindle assembly activity levels similar to those of freshly prepared extracts. Extract degradation associated with the freeze–thaw process can be substantially reduced by using centrifugal filter-based dehydration and slow sample cooling. Large amounts of frozen extract stocks from single-batch preparations allowed us to collect extensive data in micromanipulation experiments, which are often low-throughput, and thus enabled the clarification of correlations between metaphase spindle size and stiffness. Our method provides an assay platform with minimized biological variability and improves the accessibility of egg extracts for research.**

Monitoring Editor
David G. Drubin
University of California, Berkeley

Received: Mar 17, 2017
Revised: May 30, 2017
Accepted: May 31, 2017

INTRODUCTION

Proper assembly of the microtubule-based bipolar spindle is crucial for successful cell division in eukaryotes. The size of this essential subcellular structure varies across species and across cell types within species, via well-controlled biological programs (Levy and Heald, 2012; Mitchison *et al.*, 2015). For example, spindle size scales with cell size, which decreases exponentially over multiple divisions in the early stages of *Xenopus laevis* development (Wühr *et al.*, 2008). The proper spindle size ensures that chromosomes are segregated to distant locations, without perturbing the overall integrity of the cell. However, it is largely unknown how spindle size is related to other important characteristics in mitosis, such as the mechanical properties of the spindle (Dumont and Mitchison, 2009; McIntosh *et al.*, 2012; Forth and Kapoor, 2017; Kapoor, 2017).

Cell-free extracts prepared from unfertilized eggs of *X. laevis* are a model experimental system that has contributed substantially toward understanding spindle assembly and function. This system is open to a variety of biochemical manipulations, such as fractionation and immunodepletion, to identify important proteins required for proper functioning of the spindle (Murray, 1991; Desai *et al.*, 1999; Hannak and Heald, 2006). The assembled spindles can also be targeted for micromanipulation studies using cantilevers or glass microneedles, thus allowing for an examination of the structural stability of spindles against mechanical perturbations (Gatlin *et al.*, 2009, 2010; Itabashi *et al.*, 2009; Shimamoto *et al.*, 2011; Takagi *et al.*, 2013, 2014). Despite such experimental versatility, this system has several potential drawbacks. For example, the endogenous activity of extracts is retained for only a short time (typically 2–8 h from when eggs are crushed). Also, extracts exhibit great variation in quality, mostly due to egg quality and preparation processes, often resulting in considerable variation in spindle phenotypes, such as size, shape, and response to perturbations (Hannak and Heald, 2006; Grenfell *et al.*, 2016). These variations among preparations make it difficult to collect a large number of data sets within a controlled biological setting, particularly for measurements that are

This article was published online ahead of print in MBoC in Press (http://www.molbiolcell.org/cgi/doi/10.1091/mbc.E17-03-0174) on June 7, 2017.

*Address correspondence to: Yuta Shimamoto (yuta.shimamoto@nig.ac.jp).

Abbreviations used: BCA, bicinchoninic acid; DAPI, 4′,6-diamidino-2-phenylindole; ROI, region of interest.

intrinsically low throughput, that is, those that span a long period and are restricted to examinations of one sample at a time. This often masks valuable information that underlies heterogeneity of samples.

One way to overcome these problems is to prepare frozen extract stocks that retain intrinsic biochemical activity. Frozen extracts that are routinely used in laboratories are capable of reconstituting essential cell cycle events, such as DNA replication and chromosome organization, but not bipolar spindle assembly (Hannak and Heald, 2006; Gillespie *et al.*, 2012). For many years, the cryopreservation of biological materials, such as cells and tissues, has been extensively studied; the consensus is that the key to successful preparation is the prevention of ice crystal formation in the cytoplasm, which may cause significant damage to organelles and other cellular structures (Muldrew *et al.*, 2004; Fowler and Toner, 2005). A widely used technique for preventing ice crystal formation is to supplement the freezing medium with cryoprotectants, such as dimethyl sulfoxide. However, these reagents are often toxic at their effective concentrations and are difficult to remove from the cytoplasm for sample recovery (Song *et al.*, 1995). Another important technique is to freeze a sample at a slow speed (e.g., −1°C/min). This allows the liquid outside the cell to crystallize first, making the cells hypertonic; water then flows out of the cytoplasm through the cell membrane, reducing the probability of ice formation within the cell (Fowler and Toner, 2005). However, excessive dehydration causes a loss of cellular activity, because it may alter the balance of the cell's chemical composition. Additionally, frozen samples must be rehydrated for their recovery during thawing. Although such methods have been developed for cells and tissues (Kaiser, 2002; Fowler and Toner, 2005), their application to egg extracts has not been effective, owing to their cell-free nature.

Here we report a simple two-step method for preparing frozen *Xenopus* egg extract with biochemical activity retained at levels close to those of freshly prepared extracts. When a centrifugal filter membrane and a slow cooling device is used, optimal freezing conditions can be achieved without a loss of spindle assembly activity. This enabled us to repeat a large number of force measurements in bipolar metaphase spindles, which are low throughput and thus allow only a few samples to be examined in each fresh preparation. Our measurements reveal the existence of a scaling mechanism between spindle size and stiffness.

RESULTS AND DISCUSSION

Inspired by cryopreservation studies, we sought to separate the aqueous content in freshly prepared extracts in a controlled manner. To this end, we employed a centrifugal filter device, which is typically used for concentrating protein samples (Figure 1A, top). Briefly, metaphase-arrested fresh extracts were prepared according to the established protocol (Desai *et al.*, 1999) and then loaded into a filter device equipped with a 100-kDa membrane. Centrifugation at 17,000 × *g* for 10 min resulted in separation of the extract into concentrate and flow-through fractions, which were each transferred to test tubes and cooled to −80°C at approximately −1°C/min. The frozen concentrate and flow-through fractions were thawed on ice and then combined before experimental assays (Figure 1A, bottom). Upon centrifugation, the protein concentration of the extract, as determined by Bradford assay and verified by micro–bicinchoninic acid (BCA) assay, increased from 80 ± 5 mg/ml to 97 ± 10 mg/ml (mean ± SD, $n = 3$ preparations; Supplemental Figure S1A). In contrast, the flow-through fraction was ~0.25 the volume of the loaded extracts and contained only a trace amount of protein (1.8 ± 0.2 mg/ml, ~0.5% of the total protein content; Supplemental Figure S1A). The centrifugal parameters we employed here were larger in relative centrifugal force and shorter in spin time compared with those in a previous study (Wühr *et al.*, 2015) that aimed to fractionate extracts, to ensure that filtration was completed as quickly as possible. Our procedure yielded a relatively low level of protein elution into the flow-through (Supplemental Figure S1B), while the filtering capacity of the membranes was maintained nearly intact (Supplemental Figure S1, C–E). Upon recovery, the extracts had a protein concentration of 79 ± 5 mg/ml ($n = 3$), which is comparable to that of fresh extracts before centrifugation (Supplemental Figure S1A). SDS–PAGE analysis showed no prominent loss of protein content after the procedure (Supplemental Figure S1F). We refer to extracts prepared by this method as "filtered frozen extracts."

To determine how much endogenous activity was retained in the filtered frozen extracts, we ran cycled spindle assembly reaction (Desai *et al.*, 1999) and examined microtubule-based structures assembled around metaphase sperm nuclei (Figure 1, B–D). Phenotypes were analyzed in fixed squashes and compared with those of freshly prepared extracts and frozen extracts prepared without filtration; comparisons were made between extracts that originated from identical preparation batches. We found that the major fraction of sperm nuclei in filtered frozen extracts had prominent microtubule assembly activity that was close to the activity in fresh extracts, and many of the structures were bipolar (Figure 1B, left and right panels). In contrast, in nonfiltered frozen extracts, few or no such structures were observed (Figure 1B, center panel). We quantitatively analyzed microtubule assembly activity in those extracts by counting the number of sperm nuclei that exceeded a threshold level of tubulin fluorescence. The analysis was repeated with three independent preparations. We found that, in filtered frozen extracts, the fraction of sperm nuclei with a significant tubulin signal was as high as that in the fresh extracts for all three preparations (93 ± 5% vs. 89 ± 7%, mean ± SD); in contrast, in nonfiltered frozen extracts, two of the three preparations showed considerable reductions in activity (<50%) (Figure 1C). Moreover, in filtered frozen extracts, 69 ± 11% of these structures were of the typical bipolar shape with focused poles, and this was comparable to or even slightly higher than in the fresh extracts (53 ± 17%) (Figure 1D) and in those reported previously (50–80%; Budde *et al.*, 2001; Miyamoto *et al.*, 2004; Helmke and Heald, 2014). In contrast, in nonfiltered frozen extracts, only ~10% of the assembled structures were bipolar (10 ± 11%; Figure 1D). In all experimental conditions, the remaining fraction predominantly comprised monopolar, multipolar, or disorganized structures (Supplemental Figure S1G). The bipolar spindles in filtered frozen extracts maintained their overall morphology and equatorial chromosome alignment for > 20 min, indicating that the extracts retained cell cycle arrest at metaphase (Supplemental Figure S1, H and I). Therefore our filtration method significantly improves bipolar metaphase spindle assembly in frozen extracts.

To quantitatively assess the morphology of the assembled structures, we analyzed the length, width, tubulin quantity, and chromosome alignment of bipolar spindles using an automated image analysis pipeline (Grenfell *et al.*, 2016; Figure 2A and Supplemental Figure S1J). In agreement with a previous study (Grenfell *et al.*, 2016), the morphology of individual spindles in fresh extracts varied widely within each preparation (Figure 2B, left three columns), and the median values exhibited substantial variation between preparations (horizontal lines in the box charts). For example, the median spindle lengths analyzed in three independent preparations were 34.5, 43.3, and 45.4 µm ($n = 46$, 26, and 36, respectively). For quantities of other parameters, see Supplemental Table S1, upper panel. The morphological parameters analyzed for filtered frozen extract

spindles also had large variation in their distributions and median values (Figure 2B, right three columns). For example, the median spindle lengths in three independent preparations were 48.0, 43.2, and 44.9 μm (n = 30, 48, and 31, respectively). Notably, although one of the three preparations showed a relatively large difference in median spindle length between filtered frozen extracts and their original fresh extracts (39%; Figure 2B, preparation batch 1), the remaining two preparations yielded much smaller deviations in their median spindle lengths (0.2% and 1.1%; Figure 2B, preparation batches 2 and 3, respectively). Typical median spindle length variation that arises upon each fresh extract preparation is ~10–20% (e.g., 14% for n = 3 independent preparations in this study; 11%, 13%, and 17% for n = 26, 19, and 5 preparations, respectively, in studies conducted by different experimenters in Grenfell *et al.*, 2016; Supplemental Table S1, lower panel). The analysis was also performed for other spindle morphological parameters, and the differences between filtered frozen extracts and their original fresh extracts were at most approximately twofold of the SDs seen among fresh preparations (Supplemental Table S1, lower panel). Therefore variation in spindle morphology between filtered frozen extracts and their original fresh extracts, if any, is comparable to variation that arises during fresh extract preparation.

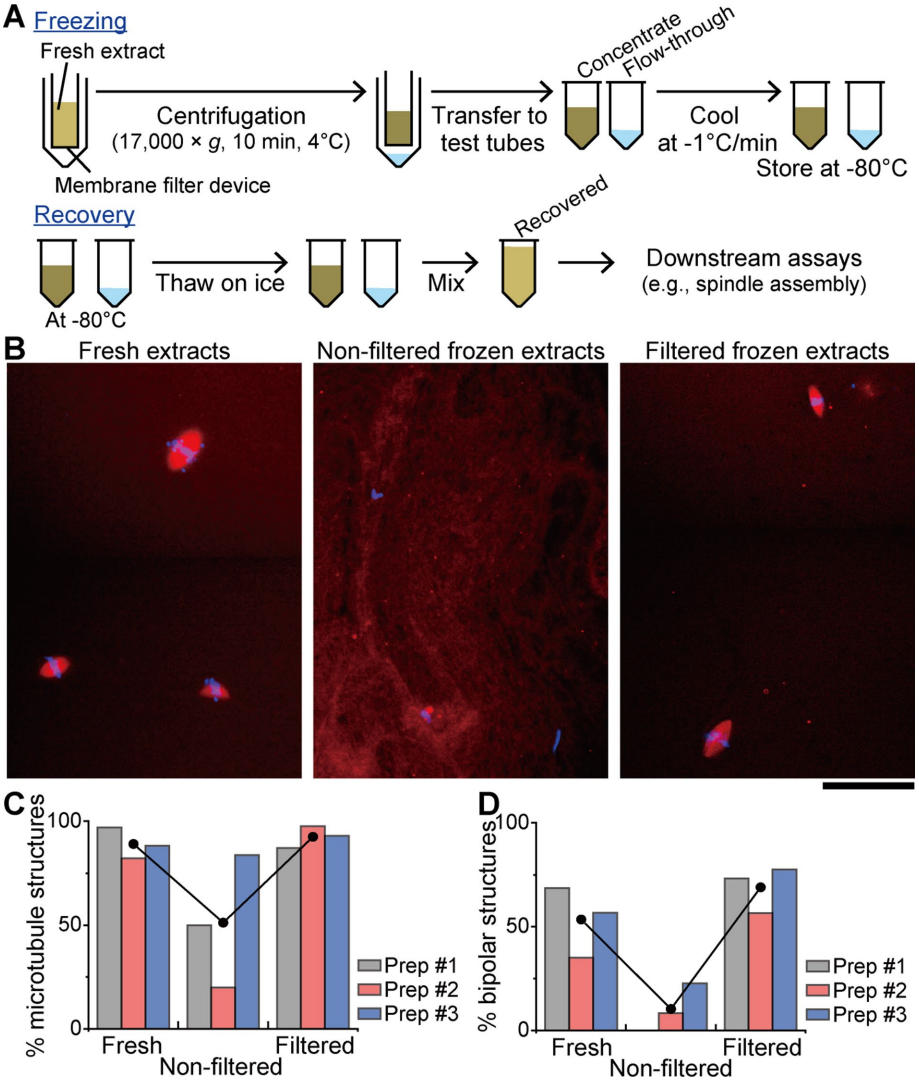

FIGURE 1: Preparation and use of frozen *Xenopus laevis* egg extracts that retain spindle assembly activity. (A) Procedure for preparing frozen *Xenopus* egg extracts that are capable of bipolar spindle assembly. For freezing, freshly prepared extracts (yellow) are loaded into the centrifugal filter device (200 μl per device) and then spun at the indicated parameters. The resultant concentrate (dark brown) and flow-through (light blue) fractions are transferred to separate test tubes and cooled to −80°C at approximately −1°C/min. For recovery, the frozen fractions are thawed on ice and then combined. (B) Representative fluorescence images of microtubule-based structures (red: tetramethylrhodamine-tubulin, 500 nM) assembled around metaphase sperm nuclei (blue: DAPI, 1 μg/ml). Freshly prepared extracts, frozen extracts prepared without filtration, and those prepared with filtration were fixed in squashes after cycling once through interphase and back into metaphase. Scale bar: 100 μm. (C) Fraction of sperm nuclei that associated with significant microtubule assembly. Data from three independent preparations are shown (colored bars). Integrated fluorescence intensity of labeled tubulins was analyzed around each sperm nucleus in fresh extracts (n = 69, 90, and 68), nonfiltered frozen extracts (n = 64, 60, and 105), and filtered frozen extracts (n = 47, 87, and 43); those that exceeded a certain threshold were scored. (D) Fraction of microtubule-based structures that were of bipolar shape, with focused poles. The structures scored in C were analyzed to examine their bipolarity (n = 67, 74, and 60 for fresh extracts; n = 32, 12, and 88 for nonfiltered frozen extracts; n = 41, 85, and 40 for filtered frozen extracts).

Successful cryopreservation requires an empirical determination of optimal parameters for dehydration, cooling, and recovery (Fowler and Toner, 2005). We therefore examined several factors that may affect the quality of frozen extract stocks. First, we examined the speed of sample cooling and found that snap freezing the concentrate fraction resulted in a significant loss of spindle assembly activity (Supplemental Figure S2, A and B). Second, we examined the speed of sample thawing and found that spindle assembly activity did not differ significantly between frozen extracts thawed on ice or at 16°C (Supplemental Figure S2, C and D). Third, we examined the requirement of extract rehydration and confirmed that the entire flow-through fraction has to be added back to the concentrate to restore endogenous activity. Without rehydration, massive microtubule polymerization occurred throughout the cytoplasm (Supplemental Figure S2, E and F). Fourth, we examined the period of centrifugation and found that it should be limited to less than 10 min. Increasing the centrifugation time resulted in a larger flow-through volume and thus more dehydration of extracts (Figure 3A). The spindle assembly activity improved accordingly, but excess centrifugation impaired extract quality (Figure 3, B and C). Finally, we compared different filter mesh sizes and found that a 100-kDa mesh is optimal. Preparation with smaller mesh sizes (e.g., 10 kDa) resulted in less protein elution in the flow through (<0.2 mg/ml vs. 1.8 mg/ml for a 100-kDa mesh). The concentration rate of extracts was consequently reduced by ~3% (Figure 3E). Although the microtubule assembly activity was nearly independent of the filter mesh

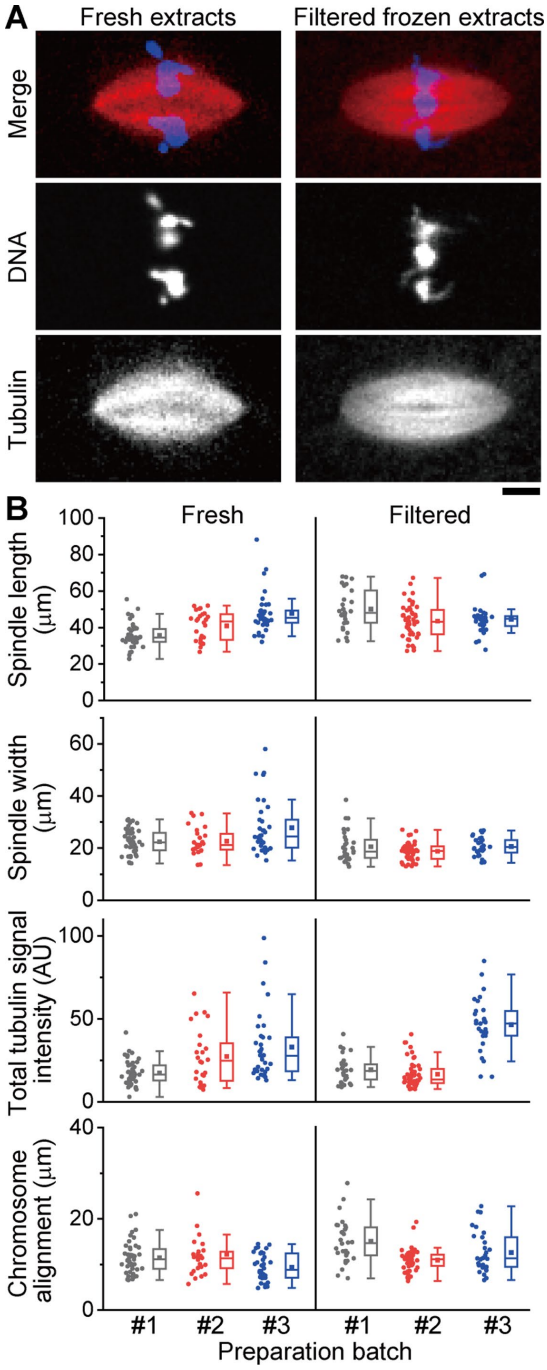

FIGURE 2: Metaphase spindle morphology in fresh and filtered frozen extracts. (A) Representative fluorescence images of bipolar metaphase spindles (red: tetramethylrhodamine-tubulin; blue: DAPI) assembled in fresh extracts or filtered frozen extracts. Scale bar: 10 μm. (B) Distributions of spindle morphological parameters. Bipolar structures scored in Figure 1D were analyzed to determine individual spindle length, width, total tubulin signal intensity, and chromosome alignment for fresh (left columns; $n = 46$, 26, and 34 spindles) and filtered frozen extracts (right columns; $n = 30$, 48, and 31 spindles) (Supplemental Figure S1J). Data from three independent preparations are shown in colored box charts with individual plots. Within the box charts, the solid squares indicate mean values, and the horizontal lines indicate median values. The bottoms and tops of the boxes indicate first and third quartiles, respectively. Whiskers show highest and lowest values within 1.5 times the interquartile range. For statistical analysis results, see Supplemental Table S1.

size (Figure 3F), bipolar spindles were more consistently formed in extracts prepared using a 100-kDa filter (Figure 3G). We note that, in contrast to the marked sensitivity of spindle assembly probability with respect to the preparation parameters, the bipolar spindle morphology was quite robust to variation in those parameters (Figure 3, D and H). Together these results highlight the importance of filtration parameters and cooling speed in our preparation procedure for assembling bipolar spindles at numbers similar to those that can be achieved in fresh extracts.

Repeating experiments with minimal sample variation requires the preparation of a sufficient amount of frozen stock and long-term maintenance of stock activity. To this end, we examined 1) the optimal preparation volume of the extract and 2) the storage stability of frozen stocks (Supplemental Figure S2, G–N). Preparation with our standard protocol (loading volume: 200 μl) consistently yielded high-quality frozen extracts compared with smaller (e.g., 100 μl) and larger (e.g., 500 μl or 1 ml) extract volumes (Supplemental Figure S2, G–K). This reduction in quality is most likely associated with the filtration step, as changes in extract volume during the freezing step did not significantly alter the probability of bipolar spindle formation (Supplemental Figure S2, L and M). Frozen stocks prepared with the optimal condition can be stored at −80°C for at least 1–10 d, and have been successful thus far for ~4 mo without significant deterioration of spindle assembly activity (Supplemental Figure S2N). Hence large-scale preparation can be achieved by processing multiple 200-μl extracts in parallel.

Upon establishing the method for preparing frozen extract stocks, we examined the mechanical response of metaphase spindles to stretching force and its dependency on overall spindle size. To this end, metaphase spindles were assembled in filtered frozen extracts and stretched using the microneedle-based setup we developed previously (Shimamoto *et al.*, 2011; Takagi *et al.*, 2014). Each measurement typically takes >10 min, and 5–10 spindles can be examined in a single spindle assembly reaction. For the acquisition of a large number of measurements (e.g., $n > 50$), the spindle assembly reaction was performed using several frozen stocks originating from a single-batch preparation (Figure 4A), and results were confirmed across three preparation batches. Figure 4B shows typical time-lapse images acquired during the measurement. In the images, a single metaphase spindle was captured using a pair of glass microneedles, the tips of which were inserted into each half of the spindle (Figure 4B, 0 s). Application of an outward stretching force, which was performed by moving the tip of one microneedle (Figure 4B, blue arrowheads) away from the other, resulted in elongation of the spindle (Figure 4B, 4 s). Tension developed across the bipolar structure, as revealed by the displacement of the force-calibrated flexible microneedle tip from the original position (Figure 4B, red arrowheads and the broken line), and increased as the spindle was stretched (Figure 4B, 8 s). The spindle pole was gradually disorganized as the stretching force increased and then eventually split apart (Figure 4B, white arrows, 12–16 s). As a result, the microneedle tip was detached from the spindle and returned to the original position (Figure 4B, 16 s). A quantitative analysis of force and spindle deformation revealed that the tension first increased in an approximately linear manner with increasing spindle length and decreasing spindle width (Figure 4C, 2–9 s) and then nearly reached a plateau before the pole was split (Figure 4C, ~11 s). On the basis of the time recordings, we generated a force-extension plot (Figure 4D), from which two mechanical properties of the spindle were determined: 1) the stiffness of the entire spindle structure, as analyzed based on a linear regression within the initial 5% range of extension (Figure 4D, red line); and 2) the mechanical strength of the spindle pole against the

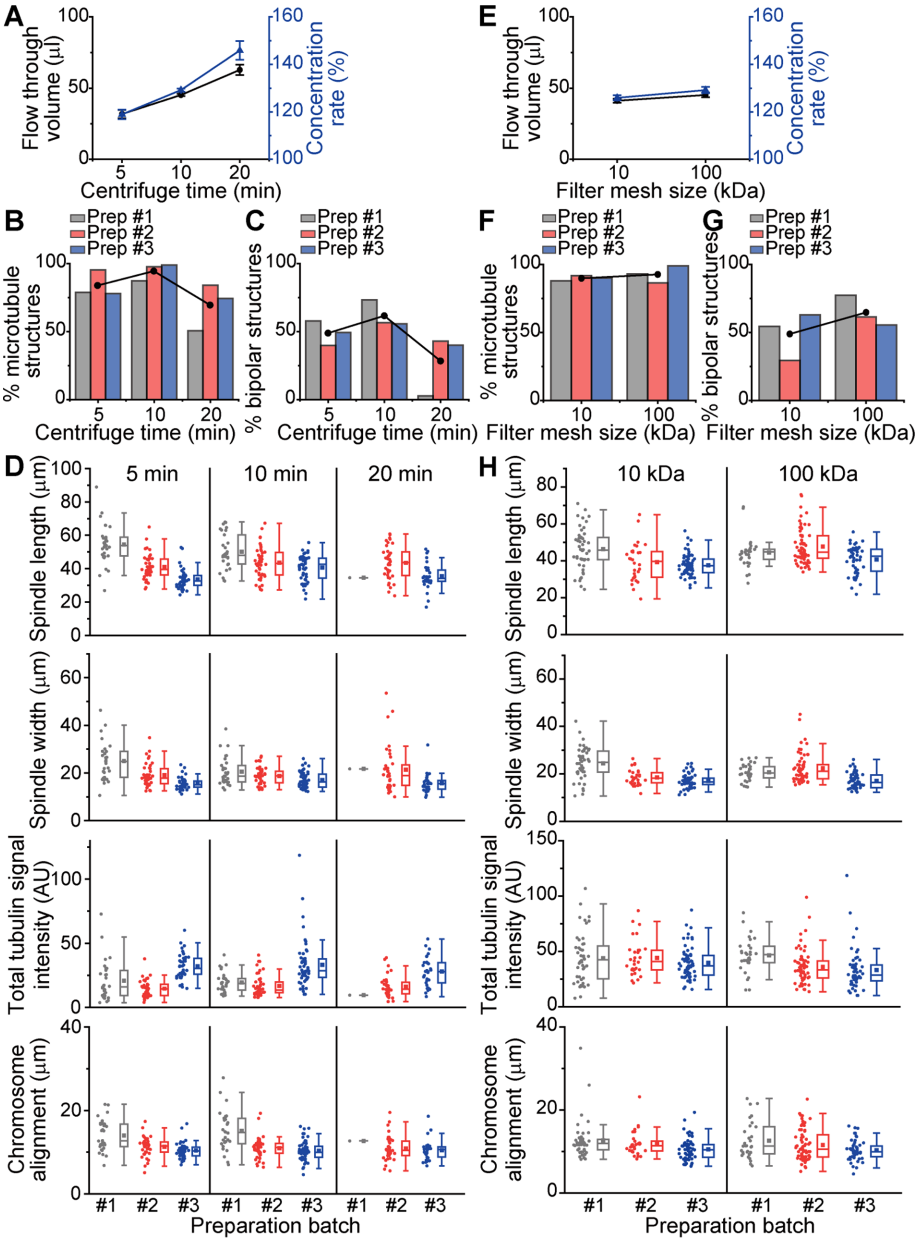

FIGURE 3: Optimization of the frozen preparation procedure. Dependencies of the spindle assembly activity of extracts on centrifugation time (A–D) and filter mesh size (E–H). Data from three independent preparations for each condition are shown (colored bars and plots). (A, E) Concentration rate (blue triangles, as a percentage of the original extract volume) estimated from the volume of flow through (black circles, in µl) obtained with indicated centrifugation time (A) or filter mesh size (E). Plots are presented as mean ± SD ($n = 3$). (B, F) Fraction of sperm nuclei that were associated with significant microtubule assembly. Analysis was performed as in Figure 1C. The structures analyzed were (B) $n = 66$, 108, and 109 for 5-min spin; $n = 47$, 87, and 98 for 10-min spin; and $n = 77$, 100, and 101 for 20-min spin, respectively; and (F) $n = 100$, 111, and 111 for 10-kDa filter and $n = 43$, 126, and 98 for 100-kDa filter, respectively. (C, G) Fraction of microtubule-based structures that were of bipolar shape with focused poles. Analysis was performed as in Figure 1D. The structures analyzed were (C) $n = 52$, 103, and 85 for 5-min spin; $n = 41$, 85, and 97 for 10-min spin; and $n = 39$, 84, and 75 for 20-min spin, respectively; and (G) $n = 88$, 102, and 100 for 10-kDa filter; and $n = 40$, 109, and 97 for 100-kDa filter, respectively. Black circles in B, C, F, and G are mean values in each preparation condition. (D, H) Distributions of spindle morphology parameters. Bipolar structures scored in C ($n = 30$, 41, and 42 for 5-min spin; $n = 30$, 48, and 54 for 10-min spin; and $n = 1$, 36, and 30 for 20-min spin, respectively) and G ($n = 48$, 30, and 63 for 10-kDa filter; and $n = 31$, 67, and 54 for 100-kDa filter, respectively) were analyzed to determine individual spindle length, width, total tubulin signal intensity, and chromosome alignment in each preparation condition. Box chart representations are as in Figure 2B.

motion of a microneedle along the long axis of the spindle, as analyzed based on the peak force that appeared near the maximum spindle extension (Figure 4D, blue line).

We repeated the measurement for 63 spindles from a single-batch preparation and found that the stiffness of the entire spindle structure was positively correlated with the initial spindle length measured before stretch (Pearson's $r = 0.41$; Figure 4E, black solid circles). We repeated this analysis with two other preparation batches and confirmed that the result was consistent (Pearson's $r = 0.48$ and 0.34, respectively, $p < 0.05$; Figure 4E, red and blue solid circles). The average spindle stiffness measured here was comparable to that observed in fresh extracts in our previous work (Takagi *et al.*, 2014). However, owing to a limited number of samples and large quality variation between preparations ($n = 14$ spindles from five fresh extract preparations), our previous work did not show statistically significant correlation between spindle size and stiffness (Figure 4E, green open circles; $r = 0.08$). The measurement in frozen preparations also revealed that the mechanical strength of the spindle pole correlated positively with the spindle length (Figure 4F; $r = 0.55$, 0.51, and 0.42, $p < 0.05$). Analyses of fluorescence imaging data further revealed that the total amount of spindle microtubules, as estimated based on the total signal intensity of dye-labeled tubulins within the bipolar structure, was greater in larger spindles (Figure 4G; $r = 0.75$, 0.70, and 0.70, $p < 0.05$). Accordingly, the measured mechanical properties of the metaphase spindle correlated with the total amount of spindle microtubules (Supplemental Figure S3; $r = 0.51$, 0.62, and 0.58 for spindle stiffness, $r = 0.49$, 0.65, and 0.62 for spindle pole strength, $p < 0.05$), but did not consistently show preferential association with either of the spindle morphology parameters (Figure 4, E and F, and Supplemental Figure S3, A and B; r values were compared for each colored plot by t test). Taken together, our assay results reveal the existence of a scaling mechanism between metaphase spindle stiffness, size, and amount of spindle microtubules.

In this study, we demonstrated the preparation and use of frozen *Xenopus* egg extracts that possess a nearly intrinsic level of spindle assembly activity. Our results predict that an optimal dehydration and slow cooling are essential parts of a successful frozen preparation, and these two steps are separable. An important biochemical activity is likely contained in the concentrate and not in the flow-through

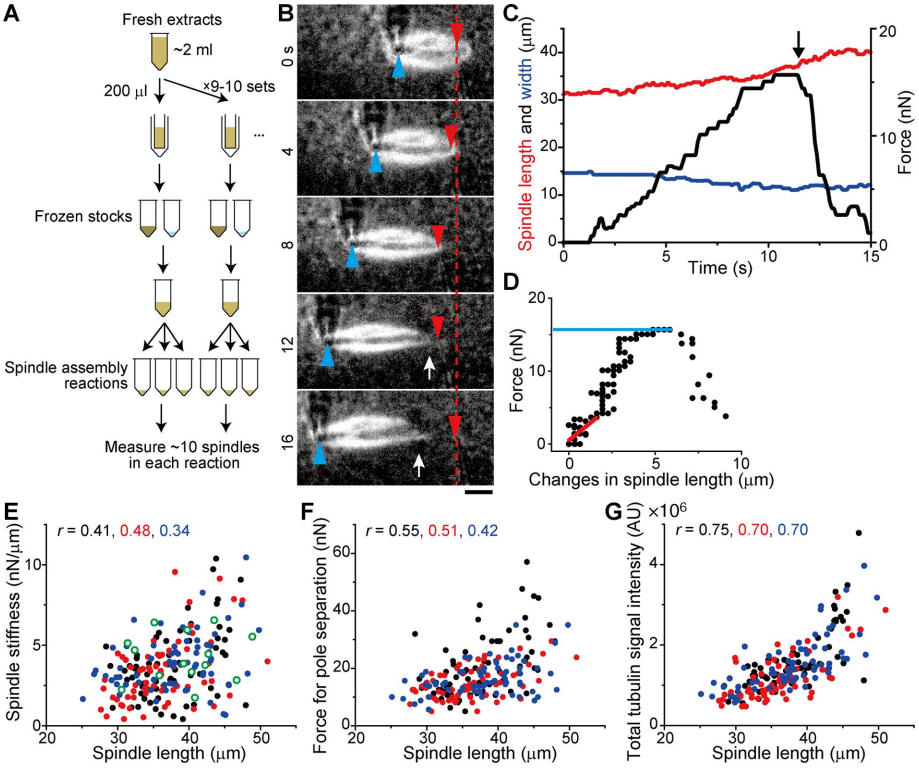

FIGURE 4: Size-dependent mechanical properties of *Xenopus* extract metaphase spindles. (A) Schematic showing the procedure for the batch preparation of filtered frozen extracts used for the assay. Freshly prepared extracts >2 ml in volume are split into aliquots (200 µl each) and subjected to frozen extract preparation, as summarized in Figure 1A. Each frozen stock is thawed for recovery just before use. Data from several days of experiments performed with the same preparation batch are pooled and analyzed. The typical number of measurements acquired per each spindle assembly reaction is ~10. (B) Time-lapse images of a bipolar metaphase spindle assembled in filtered frozen extracts and stretched by a dual microneedle-based setup. Confocal fluorescence (tetramethylrhodamine-labeled tubulin, 500 nM) and bright-field images acquired simultaneously during the time-lapse are overlaid (time stamp: in seconds). In the images, the manipulation microneedle tip (marked in blue) was moved at 2 µm/s. Tension that developed across the spindle was monitored based on the displacement of the force-sensing flexible microneedle tip (marked in red, stiffness: 1.9 nN/µm) from its equilibrium (dashed line). White arrows highlight disorganization and breakage of the spindle pole. Scale bar: 10 µm. (C) Changes in spindle length (red), width (blue), and magnitude of force (black) analyzed in B over time. The black arrow indicates the time at which the spindle pole was split apart. (D) Force-extension plots. Changes in spindle length during the time course in **C** are plotted against the magnitude of developed force. Linear regression was performed within a 5% extension range (red solid line) to determine the stiffness of the entire spindle structure. Plateau of the force-extension plot (blue solid line) was used to determine the pole-splitting force. (E, F) Dependencies of spindle stiffness (E) and pole-splitting force (F) on spindle size. A total of $n = 65$, 66, and 67 spindles were examined in three independent preparations (black, red, and blue solid circles, respectively) and plotted against each spindle length measured before microneedle insertion. Green open circles in E are data obtained in fresh extracts ($n = 14$ spindles from five independent preparations) (Takagi *et al.*, 2014). (G) Dependencies of spindle microtubule amount on spindle size. Integrated fluorescence signal intensity of dye-labeled tubulin within each spindle was analyzed for the data set in E and F. The tubulin images acquired before micromanipulation procedure were used for analysis. Top left *r* values in E–G are Pearson correlation coefficients analyzed for each data set.

fraction, as spindle assembly activity depended strongly on the concentrate when those two fractions from independent preparations were interchanged (Supplemental Figure S1K). Along with analyses of cytoplasmic structure and composition, our study should help elucidate the molecular basis underlying biological sample freezing.

The mechanical measurement using our frozen extract stocks provides important insights into how different-sized metaphase spindles respond to external force. If we assume that the local elasticity of a spindle per unit length is constant and these units are connected in series along the pole-to-pole axis of the spindle, the total stiffness of the spindle should be inversely proportional to the spindle length. Our measurement reveals that the relationship is the opposite. We previously reported that the three-dimensional volume of *Xenopus* extract spindles increases exponentially with spindle length while the aspect ratio of the bipolar structure is maintained (Takagi *et al.*, 2013). One plausible explanation is that this allometric effect allows for an integrated conjugation of local elastic units on both the long and short axes of the spindle, leading to the size-dependent increase of overall spindle stiffness. The spindle has an ability to dynamically change its size and shape in response to physical and biochemical perturbations (Dumont and Mitchison, 2009; Mitchison *et al.*, 2015; Levy and Heald, 2016; Kapoor, 2017). The scaling mechanism we found here suggests an additional functional importance of controlling the spindle size: to maintain the mechanical stability of this essential cytoskeletal structure.

Since its development and first use (Lohka and Masui, 1983), the *Xenopus* extract system has contributed to the discovery of many essential proteins and pathways for cell cycle events (Hannak and Heald, 2006; Cross and Powers, 2009: Gillespie *et al.*, 2012). Our present method provides a platform for obtaining variable information with minimal sample heterogeneity and offers a supply source for researchers. We anticipate that these features will allow the extract system to be expanded for broader use in the scientific community.

MATERIALS AND METHODS

Preparation of *Xenopus* egg extracts

Cell-free extracts from unfertilized *Xenopus laevis* eggs arrested at metaphase were prepared as described previously (Desai *et al.*, 1999), except that Energy Mix was used at 50× instead of 20×. For the preparation of filtered frozen extracts, freshly prepared extracts were loaded into centrifugal filter devices (200 µl per device; UFC510024; Millipore) and spun at 17,000 × *g* for 10 min at 4°C using a tabletop centrifuge (5424R; Eppendorf). The filtration was completed within 30 min after fresh extract preparation, as a prolonged incubation markedly reduced the quality of frozen extract stocks. Following centrifugation, the filter devices were placed upside down in collection tubes and spun at 2000 × *g* for ~10 s (Multi Spin; TOMY) to transfer the concentrate to the tubes. The concentrate and flow-through fractions were then transferred to separate 1.5-ml test tubes by using low-adhesion pipette tips. The tubes were placed in a tube cooler (Chillette 12;

Denville Scientific), which was precooled to 4°C, and frozen at a cooling rate of approximately −1°C/min in a −80°C freezer. Before the spindle assembly reaction, the frozen concentrate and flow-through fractions were thawed on ice and then combined by reintroducing the entire flow-through fraction to the concentrate fraction. The recovered extracts were used for assays following > 20 min of incubation on ice. Nonfiltered frozen extracts, which were used as controls in Figure 1, were prepared in the same manner as above, but without centrifugal filtration. For a part of the analysis shown in Figure 3, E–H, filter devices of a smaller mesh size (UFC501024; Millipore) were used. For the analysis shown in Supplemental Figure S2K, filter devices of a larger volume capacity (UFC210024; Millipore) and modified centrifugal parameters (5400 × *g*, 31 min) were used. The entire procedure was performed while keeping extract samples on ice as much as possible. Sample handling was performed using wide-bore pipette tips, which were prepared by cutting off the ends with a razor blade.

Preparation of spindle samples

Metaphase spindles were assembled by cycling the extracts with demembranated *X. laevis* sperm nuclei (~400 nuclei/μl) once through interphase and back into metaphase (Desai *et al.*, 1999). Each reaction was performed in a 20-μl volume at 16°C in 1.5-ml test tubes. Fixed samples were prepared 90 min after the start of spindle assembly, each with 4 μl of fixation buffer (125 mM HEPES, 2.5 mM EDTA, 2.5 M NaCl, 50 mM KCl, 25 mM $MgCl_2$, 50 mM $CaCl_2$, 10% formaldehyde, 60% glycerol, and 1 μg/ml 4′,6-diamidino-2-phenylindole [DAPI]) and 2 μl of extract reaction supplemented with 500 nM tetramethylrhodamine-tubulin, squashed between a clean slide and a 18 × 18 mm coverslip. Live spindle samples for micromanipulation experiments were prepared by performing the cycling reaction as described above, but with 500 nM tetramethylrhodamine-tubulin and 250 nM SYTOX Green.

Force-measurement assays

Mechanical properties of extract spindles were examined using the microneedle-based setup we developed previously (Shimamoto *et al.*, 2011; Takagi *et al.*, 2014). Metaphase extracts containing preassembled spindles (volume: 4 μl) were placed on a passivated coverslip and covered with mineral oil. The coverslips used were siliconized and precoated with Pluronic F-127 (Gatlin *et al.*, 2010). A pair of force-calibrated microneedles, which were prepared according to a previously described method (Shimamoto and Kapoor, 2012) and were each held by three-axis micromanipulators (MHW-3; Narishige), were inserted into each half of a single bipolar spindle. The tip of one microneedle was sufficiently stiff (>1000 nN/μm) to allow for the controlled micromanipulation of spindles, whereas the tip of the other microneedle was much more flexible (stiffness $k = 1.9$ nN/μm) to measure the amount of applied force. The mechanical strengths of the entire spindle structure and its poles were examined by moving the stiff microneedle away from the flexible microneedle along the spindle's pole-to-pole axis at 2 μm/s. The microneedle motion was controlled using a closed-loop piezo driver (E-665; Physik Instrumente) and a piezo actuator (P-841.20; Physik Instrumente) attached to the microneedle's base. The measurements were performed in a temperature-controlled room at 18 ± 1°C and completed within 60 min after spindle assembly, over which no detectable changes in spindle mechanics and morphology were observed without micromanipulation.

Microscopy

Fluorescence imaging of extract samples was performed using an inverted microscope (Ti; Nikon) equipped with a 20× objective lens (Plan-Apo, 0.75NA; Nikon), a piezo-driven objective scanner (P-725.4CD, PI), an sCMOS camera (Neo 4.1; Andor), a motorized X-Y stage (MS-2000; Applied Scientific Instrumentation), an epifluorescence illuminator (Intensilight; Nikon), and a spinning-disk confocal unit (CSU-X1; Yokogawa). The epi-illuminator was used with fluorescence filter sets (TxRed-4040C-000 and DAPI-1060B-000; Semrock) to acquire images of fixed samples. The spinning-disk confocal unit was used with two diode lasers (488 and 561 nm; OBIS; Coherent) for live spindle imaging. The entire microscope system was connected to a computer for automated image acquisition using NIS-Elements software (version 4.50; Nikon). Fixed samples were subjected to raster scanning to obtain large images (~10 × ~11 mm area per chamber). Live spindle samples were subjected to confocal fluorescence imaging in a streaming mode (exposure time: 100 ms).

Biochemical characterization

The protein concentration of extracts was determined using the Bradford assay (#500-0006; Bio-Rad) or the micro-BCA assay (#23235; Thermo) calibrated with the bovine serum albumin standard. The overall protein composition of extracts was analyzed by SDS–PAGE (4–12% Tris-glycine, Invitrogen) and Coomassie blue staining (SimplyBlue SafeStain; Invitrogen), according to the manufacturer's protocol. A gel image was acquired using an automated gel-imaging instrument (Gel Doc EZ Gel Documentation System; Bio-Rad).

The filtration capacity of centrifugal devices was examined by analyzing the degree of protein elution using two reference proteins: ovalbumin (A5503; Sigma-Aldrich; 3.0 mg/ml) and cytochrome c (C2506; Sigma-Aldrich; 6.4 mg/ml) diluted in CSF-XB (100 mM KCl, 0.1 mM $CaCl_2$, 2 mM $MgCl_2$, 10 mM HEPES, 5 mM EGTA, and 50 mM sucrose, pH 7.8). Each protein solution or a CSF-XB control (500 μl) was loaded into filter devices that had been used for filtering extract preparations and centrifuged at 17,000 × *g* for 10 min at 4°C using a tabletop centrifuge (5424R; Eppendorf). The protein concentration in each flow-through fraction was determined by the Bradford assay.

Data analysis

Classification of spindle phenotypes, that is, bipolar, monopolar, multipolar, or disorganized structure, was performed using ImageJ (version 1.49p) by visual inspection of microtubule images acquired around metaphase sperm nuclei in fixed squashes. Quantitative analysis of spindle morphological parameters was performed using a previously published image analysis pipeline (Grenfell *et al.*, 2016). Large aggregates of DNA signals were excluded from analyses.

Spindle length and width in micromanipulation experiments were determined using fluorescence time-lapse images of microtubules by performing line-scan analyses (line width = 1.6 μm) along the spindle's long axis and short axis. A typical line-scan profile exhibited a bell-like shape with a flattened top, from which the edges of the spindle structure were determined at the single pixel resolution by referencing a manually defined threshold that was set at a constant value across the time-lapse images. The magnitude of developed force (F) was determined based on the displacement of the force-calibrated microneedle's tip from its equilibrium position (Δx), according to $F = k \cdot \Delta x$, where k is the stiffness of the microneedle tip.

Stiffness of the metaphase spindle was determined based on the relationship between the magnitude of force and the change in spindle length, which was estimated by performing a linear regression analysis within the initial 5% increment of spindle length. The mechanical strength of metaphase spindle poles was determined based on the relationship between the force and the spindle length

change, which typically showed a gradual rise, followed by a sudden drop, forming a single peak in response to a constant motion of microneedle-based stretch. The magnitude of force was determined at the peak position in the force-extension plot, at which point spindle poles showed visible splitting or breakage in fluorescence time-lapse images.

The amount of spindle microtubules in micromanipulation experiments was estimated using fluorescence images of microtubules acquired before microneedle insertion. In images acquired for each spindle, a small ROI (region of interest; ~50 × ~50 µm) and a larger ROI (~100 × ~100 µm) were drawn to cover the entire spindle structure. The area and total tubulin signal intensity in the small ROI (S_{small} and I_{small}, respectively) and those in the large ROI (S_{large} and I_{large}, respectively) were then obtained. The total tubulin signal intensity in the spindle structure ($I_{spindle}$) was determined using these parameter values, according to $I_{spindle} = I_{small} - I_{bg} = I_{small} - S_{small} \cdot (I_{large} - I_{small})/(S_{large} - S_{small})$. Here I_{bg} is the total background signal intensity in the small ROI, which was estimated based on the signal intensity within the large ROI, but outside the small ROI.

Statistical analyses using Pearson correlation analysis (Figure 4, E–G, and Supplemental Figure S3, A and B) were performed in Origin 2016. For comparison of Pearson correlation *r* values (Figure 4, E and F, and Supplemental Figure S3, A and B), a statistical test described in Steiger (1980) was used.

ACKNOWLEDGMENTS

We thank Masato Kanemaki (National Institute of Genetics) for kindly sharing instruments for method optimization and Akatsuki Kimura and members of his laboratory (National Institute of Genetics) for helpful discussions. We also thank anonymous referees for their invaluable input. This work was supported by a postdoctoral fellowship of the Japan Society for the Promotion of Science (JSPS) for Young Scientists (J.T.), JSPS KAKENHI grant numbers 16H06166 and 15K14515, and PRIME, Japan Agency for Medical Research and Development (AMED) (Y.S.).

REFERENCES

Budde PP, Kumagai A, Dunphy WG, Heald R (2001). Regulation of Op18 during spindle assembly in *Xenopus* egg extracts. J Cell Biol 153, 149–158.

Cross MK, Powers MA (2009). Learning about cancer from frogs: analysis of mitotic spindles in *Xenopus* egg extracts. Dis Model Mech 2, 541–547.

Desai A, Murray A, Mitchison TJ, Walczak CE (1999). The use of *Xenopus* egg extracts to study mitotic spindle assembly and function in vitro. Methods Cell Biol 61, 385–412.

Dumont S, Mitchison TJ (2009). Force and length in the mitotic spindle. Curr Biol 19, R749–R761.

Forth S, Kapoor TM (2017). The mechanics of microtubule networks in cell division. J Cell Biol 216, 1525–1531.

Fowler A, Toner M (2005). Cryo-injury and biopreservation. Ann NY Acad Sci 1066, 119–135.

Gatlin JC, Matov A, Danuser G, Mitchison TJ, Salmon ED (2010). Directly probing the mechanical properties of the spindle and its matrix. J Cell Biol 188, 481–489.

Gatlin JC, Matov A, Groen AC, Needleman DJ, Maresca TJ, Danuser G, Mitchison TJ, Salmon ED (2009). Spindle fusion requires dynein-mediated sliding of oppositely oriented microtubules. Curr Biol 19, 287–296.

Gillespie PJ, Gambus A, Blow JJ (2012). Preparation and use of *Xenopus* egg extracts to study DNA replication and chromatin associated proteins. Methods 57, 203–213.

Grenfell AW, Strzelecka M, Crowder ME, Helmke KJ, Schlaitz AL, Heald R (2016). A versatile multivariate image analysis pipeline reveals features of *Xenopus* extract spindles. J Cell Biol 213, 127–136.

Hannak E, Heald R (2006). Investigating mitotic spindle assembly and function in vitro using *Xenopus laevis* egg extracts. Nat Protoc 1, 2305–2314.

Helmke KJ, Heald R (2014). TPX2 levels modulate meiotic spindle size and architecture in *Xenopus* egg extracts. J Cell Biol 206, 385–393.

Itabashi T, Takagi J, Shimamoto Y, Onoe H, Kuwana K, Shimoyama I, Gaetz J, Kapoor TM, Ishiwata S (2009). Probing the mechanical architecture of the vertebrate meiotic spindle. Nat Methods 6, 167–172.

Kaiser J (2002). New prospects for putting organs on ice. Science 295, 1015–1015.

Kapoor TM (2017). Metaphase spindle assembly. Biology (Basel) 6, 8.

Levy DL, Heald R (2012). Mechanisms of intracellular scaling. Annu Rev Cell Dev Biol 28, 113–135.

Levy DL, Heald R (2016). Biological scaling problems and solutions in amphibians. Cold Spring Harb Perspect Biol 8, a019166.

Lohka MJ, Masui Y (1983). Formation in vitro of sperm pronuclei and mitotic chromosomes induced by amphibian ooplasmic components. Science 220, 719–721.

McIntosh JR, Molodtsov MI, Ataullakhanov FI (2012). Biophysics of mitosis. Q Rev Biophys 45, 147–207.

Mitchison TJ, Ishihara K, Nguyen P, Wühr M (2015). Size scaling of microtubule assemblies in early *Xenopus* embryos. Cold Spring Harb Perspect Biol 7, a019182.

Miyamoto DT, Perlman ZE, Burbank KS, Groen AC, Mitchison TJ (2004). The kinesin Eg5 drives poleward microtubule flux in *Xenopus laevis* egg extract spindles. J Cell Biol 167, 813–818.

Muldrew K, Acker JP, Elliott JA, McGann LE (2004). The water to ice transition. In: Life in the Frozen State, ed. BJ Fuller, N Lane, and EE Benson, Boca Raton, FL: CRC Press, 67–108.

Murray AW (1991). Cell cycle extracts. Methods Cell Biol 36, 581–605.

Shimamoto Y, Kapoor TM (2012). Microneedle-based analysis of the micromechanics of the metaphase spindle assembled in *Xenopus laevis* egg extracts. Nat Protoc 7, 959–969.

Shimamoto Y, Maeda YT, Ishiwata S, Libchaber AJ, Kapoor TM (2011). Insights into the micromechanical properties of the metaphase spindle. Cell 145, 1062–1074.

Song YC, Pegg DE, Hunt CJ (1995). Cryopreservation of the common carotid artery of the rabbit: optimization of dimethyl sulfoxide concentration and cooling rate. Cryobiology 32, 405–421.

Steiger JH (1980). Tests for comparing elements of a correlation matrix. Psychol Bull 87, 245–251.

Takagi J, Itabashi T, Suzuki K, Kapoor TM, Shimamoto Y, Ishiwata S (2013). Using micromanipulation to analyze control of vertebrate meiotic spindle size. Cell Rep 5, 44–50.

Takagi J, Itabashi T, Suzuki K, Shimamoto Y, Kapoor TM, Ishiwata S (2014). Micromechanics of the vertebrate meiotic spindle examined by stretching along the pole-to-pole axis. Biophys J 106, 735–740.

Wühr M, Chen Y, Dumont S, Groen AC, Needleman DJ, Salic A, Mitchison TJ (2008). Evidence for an upper limit to mitotic spindle length. Curr Biol 18, 1256–1261.

Wühr M, Güttler T, Peshkin L, McAlister GC, Sonnett M, Ishihara K, Groen AC, Presler M, Erickson BK, Mitchison TJ, Kirschner MW, Gygi SP (2015). The nuclear proteome of a vertebrate. Curr Biol 25, 2663–2671.